

**PLUG-AND-PLAY UNPLUGGED:  
OPTIMIZATION FREE RECONSTRUCTION USING  
CONSENSUS EQUILIBRIUM \***

GREGERY T. BUZZARD<sup>†</sup>, SUHAS SREEHARI<sup>‡</sup>, AND CHARLES A. BOUMAN<sup>‡</sup>

**Abstract.** Regularized inversion methods for image reconstruction are used widely due to their tractability and their ability to combine complex physical sensor models with useful regularity criteria. Such methods were used in the recently developed Plug-and-Play prior method, which provides a framework to use advanced denoising algorithms as regularizers in inversion. However, the need to formulate regularized inversion as the solution to an optimization problem severely limits both the expressiveness of possible regularity conditions and the variety of provably convergent Plug-and-Play denoising operators.

In this paper, we introduce the concept of consensus equilibrium (CE), which generalizes regularized inversion to include a much wider variety of regularity operators without the need for an optimization formulation. Consensus equilibrium is based on the solution of a set of equilibrium equations that balance data fit and regularity. In this framework, the problem of MAP estimation in regularized inversion is replaced by the problem of solving these equilibrium equations, which can be approached in multiple ways, including as a fixed point problem that generalizes the ADMM approach used in the Plug-and-Play method.

We present the Douglas-Rachford (DR) algorithm for computing the CE solution as a fixed point and prove the convergence of this algorithm under conditions that include denoising operators that do not arise from optimization problems and that may not be nonexpansive. We give several examples to illustrate the idea of consensus equilibrium and the convergence properties of the DR algorithm and demonstrate this method on a sparse interpolation problem using electron microscopy data.

**Key words.** Plug and play, regularized inversion, ADMM, tomography, denoising, MAP estimate.

**AMS subject classifications.** 94A08, 68U10

**1. Introduction.** Over the past 30 years, statistical inversion has evolved from an interesting theoretical idea to a proven practical approach. Most statistical inversion methods are based on the maximum a posteriori (MAP) estimate, or more generally regularized inversion, since this approach balances computational complexity with achievable image quality. Regularized inversion is based on the solution of an optimization problem with the form

$$(1) \quad x^* = \arg \min_x \{f(x) + h(x)\},$$

where  $f$  is the data fidelity function and  $h$  is the regularizing function. In the special case of MAP estimation,  $f$  represents the forward model given by

$$f(x) = -\log p_f(y|x),$$

where  $y$  is the data and  $x$  is the unknown to be recovered, and  $h$  represents the prior model given by

$$h(x) = -\log p_p(x).$$

The solution of equation (1) balances the goals of fitting the data while also regularizing this fit according to the prior.

---

\*Submitted to the editors March 23, 2017.

**Funding:** G.T.B. was partially supported by NSF grant NSF DMS-1318894. S.S. and C.A.B. were supported by an AFOSR/MURI grant #FA9550-12-1-0458, by UES Inc. under the Broad Spectrum Engineered Materials contract, and by the Electronic Imaging component of the ICMD program of the Materials and Manufacturing Directorate of the Air Force Research Laboratory, Andrew Rosenberger, program manager.

<sup>†</sup>Department of Mathematics, Purdue University, West Lafayette, IN, USA ([buzzard@purdue.edu](mailto:buzzard@purdue.edu))

<sup>‡</sup>School of Electrical and Computer Engineering, Purdue University, West Lafayette, IN, USA ([ssreehar@purdue.edu](mailto:ssreehar@purdue.edu) and [bouman@purdue.edu](mailto:bouman@purdue.edu))

While regularized inversion is attractive, it is also limiting. For example, many of the best denoising algorithms cannot be put into the form of a simple optimization [2, 5]. Nonetheless, traditional denoising is a special case of an inverse problem in which the observed image is corrupted by additive Gaussian noise. Therefore, denoising is an example of an inverse problem that is best solved outside the restrictive framework of equation (1). This strongly suggests that more general classes of inverse problems can benefit from a generalization of regularized inversion.

Recently, a number of authors have built on the Plug-and-Play method as a way to construct implicit prior models through the use of denoising operators [17, 18, 15, 13, 16]. The goal of the Plug-and-Play method is to replace the prior model in the Bayesian formulation with a denoising operator. In [15], conditions are given on the denoising operator that will ensure it is a proximal mapping, so that the MAP estimate exists and the algorithm converges. However, these conditions impose relatively strong symmetry conditions on the denoising operator that may not occur in practice.

The paper [12] provides a different approach to building on the idea of Plug and Play. That paper uses the classical forward model plus prior model in the framework of optimization, but constructs a prior term directly from the denoising engine; this is called Regularization by Denoising (RED). For a denoiser  $x \mapsto H(x)$ , the prior term is given by  $\lambda x^T(x - H(x))$ . This approach produces an optimization problem associated with any denoiser, but in the case that the denoiser itself is obtained from a prior, the RED prior is different from the denoiser prior. Under certain conditions, one of which requires the denoiser to be nonexpansive, this optimization is convex. They also describe several algorithms for approximating a minimum, including gradient descent, ADMM, and finding a 0 of the gradient. In their examples, ADMM produces the fastest convergence among the algorithms they consider.

In this paper, we introduce a generalization of the regularized inverse that we call the consensus equilibrium (CE). The CE generalizes the concept of Plug-and-Play and the MAP estimate to cases in which there is no well-defined cost function to minimize. Instead, the CE is defined as the solution to a set of equilibrium equations, rather than the minimum of a cost function. More specifically, the CE solution seeks to balance the effect of the denoising operator with the effect of the proximal map that enforces data fidelity. When this balance is met, then the denoising operator removes precisely the same noise as is added back by the data fidelity proximal map of the Plug-and-Play method.

We first show that the consensus equilibrium is a generalization of the MAP estimate or more generally of regularized inversion. When the forward and denoising operators are proximal mappings associated with the forward and prior models, then the consensus equilibrium is exactly the MAP estimate and also the solution obtained with Plug-and-Play. However, the consensus equilibrium can still exist in the more general case when the denoising operator is not a proximal mapping. In this case, the solution has the interpretation of achieving the best denoised inverse of the data. That is, the proximal map associated with the forward model pulls the current point towards a more accurate fit to data, while the denoising operator pulls the current point towards a “less noisy” image. We illustrate this in a toy example in two dimensions: the consensus equilibrium is given by a balance between competing forces.

In addition to introducing the CE equations, we discuss ways to solve them. We propose a family of Douglas-Rachford (DR) algorithms for computing the solution to the equilibrium equations, and we provide technical conditions for provable convergence. In addition, we show that the ADMM algorithm with variable splitting as used in [15] is a special case of this more general class of algorithms. Finally, we present some experimental results that demonstrate the value of the method by applying it to inverse problems with a denoising operator based on BM3D [5].

**2. Consensus Equilibrium.** In this section, we introduce the concept of *consensus equilibrium*. In order to do this, let  $F$  and  $H$  each be maps  $\mathbb{R}^n \rightarrow \mathbb{R}^n$ . Then the consensus equilibrium is defined as any solution  $(x^*, u^*)$  that solves the equations

$$(2) \quad F(x^* - u^*) = x^*$$

$$(3) \quad H(x^* + u^*) = x^* .$$

In order to understand why the solution to this set of equations is important, first consider the special case in which  $F$  and  $H$  are proximal mappings given by

$$(4) \quad F(x) = \arg \min_v \left\{ \frac{\|x - v\|^2}{2\sigma^2} + f(v) \right\}$$

$$(5) \quad H(x) = \arg \min_v \left\{ \frac{\|x - v\|^2}{2\sigma^2} + h(v) \right\} ,$$

where  $f : \mathbb{R}^n \rightarrow \mathbb{R} \cup \{+\infty\}$  and  $h : \mathbb{R}^n \rightarrow \mathbb{R} \cup \{+\infty\}$  are proper, closed, convex functions, and  $\sigma > 0$ . Intuitively,  $f$  and  $h$  represent the forward model and regularizing function for some regularized inverse problem as in equation (1). Note that we allow for the possibility that  $h$  enforces some hard constraints by taking on the value  $+\infty$ .

In the setting of proximal maps as above, the solutions to the regularized inversion problem of equation (1) are exactly the solutions to the consensus equilibrium problem of (2) and (3). The proof is contained in Appendix A.

**THEOREM 1. (Consensus equilibrium as optimization)** *Let  $f$  and  $h$  be proper, closed, convex functions on  $\mathbb{R}^n$ . Assume  $f + h$  is finite on some open set in  $\mathbb{R}^n$ , and let  $F$  and  $H$  be the proximal maps as in (4) and (5). Then the set of solutions to the consensus equilibrium equations of (2) and (3) is exactly the set of solutions to minimization problem (1).*

**2.1. Beyond optimization.** The result above indicates that the CE equations give a solution of the regularized inverse problem in the case of proximal maps, but in fact, the CE formulation is much more general because it applies even when  $F$  and  $H$  are not proximal mappings and there is *no underlying optimization problem to be solved*.

For an interpretation beyond optimization, imagine that  $H$  is a general denoising operator such as NLM [2] or BM3D [5]. In this case, there is in general no function  $h(x)$  that produces  $H$  as a proximal map, so the regularized inversion of equation (1) no longer has any meaning, and consequently, there is no MAP estimate. Nonetheless, it may still be possible to solve the consensus equilibrium equations. In this case, the CE equations  $F(x^* - u^*) = x^*$ ,  $H(x^* + u^*) = x^*$  have the following interpretation:

- $x^*$  is the estimated signal,
- $u^*$  is the estimated noise,
- $H(x^* + u^*) = x^*$  removes noise to recover the signal,
- $F(x^* - u^*) = x^*$  adds back noise to fit the measured data.

Below we give conditions on  $F$  and  $H$  so that the consensus equilibrium equations have a solution even when there is no underlying optimization problem to be solved and describe an algorithm to compute the solution. We also give several examples.

We note that the CE formulation generalizes the Plug-and-Play reconstruction method [17] in that CE agrees with Plug-and-Play when the latter converges. So in the optimization setting, CE encompasses the original method, which yields high quality solutions for important applications in tomography [15] and denoising [13]. However, CE has the advantage that it applies to a larger class of denoising operators than the original method and is amenable to a wider variety of solution algorithms.

**3. Solving the Equilibrium Equations.** In order to solve the consensus equilibrium equations, we first transform them to a less intuitive but more tractable form. The transformed equations are derived by introducing new variables  $w^* = x^* - u^*$  and  $v^* = x^* + u^*$ , which converts the CE equations to

$$(6) \quad F(w^*) = \frac{w^* + v^*}{2}$$

$$(7) \quad H(v^*) = \frac{w^* + v^*}{2}.$$

Our strategy is first to compute the solution to these transformed equilibrium equations and then to invert the solution to get  $x^* = (v^* + w^*)/2$ ,  $u^* = (v^* - w^*)/2$ .

We next present a theorem that characterizes the solutions to the CE equations as the fixed points to the mapping  $T = (2F - I)(2H - I)$ , where  $I$  denotes the identity map, and juxtaposition of maps denotes composition.

**THEOREM 2.** *The vectors  $x^* = (v^* + w^*)/2$  and  $u^* = (v^* - w^*)/2$  give a solution of the CE equations (2) and (3) if and only if  $v^*$  is a fixed point of the map  $T = (2F - I)(2H - I)$  and  $w^* = (2H - I)v^*$ .*

*Proof.* Assume  $x^*$  and  $u^*$  are solutions of the original CE equations. The invertible linear transformation to  $w^*$  and  $v^*$  gives the equivalent form in (6) and (7), which can also be written in the form

$$(8) \quad v^* = 2F(w^*) - w^*$$

$$(9) \quad w^* = 2H(v^*) - v^*.$$

The second expression gives  $w^* = (2H - I)v^*$ , and substituting the second expression into the first gives

$$v^* = (2F - I)(2H - I)v^*,$$

so that  $v^*$  is a fixed point of  $T$  as claimed. The converse is obtained by starting with this final line and using  $w^* = (2H - I)v^*$  to reverse the steps to obtain (6) and (7), which are equivalent to (2) and (3).  $\square$

With this reformulation, we see that there are two natural approaches to finding a solution to the CE equations. One is to use root finding methods to solve (6) and (7) directly, and the other is to use iterative methods to find a fixed point of  $T$ .

In Section 3.1, we use this second approach to give a simple yet powerful method for solving the CE equations under fairly common conditions. This method is based on the Douglas-Rachford splitting algorithm, and is actually a one-parameter family of methods that agrees with ADMM for one particular choice of this parameter. This method is guaranteed to converge globally when the map  $T = (2F - I)(2H - I)$  is nonexpansive, which includes the case that both  $F$  and  $H$  are proximal maps for convex functions but also includes cases when this is not true.

In Section 3.2, we relax the conditions on  $T$  to ensure convergence for a larger class of  $F$  and  $H$ , although in this case we are able to give only local convergence conditions. We also mention briefly some possible approaches based on solving the CE equations with root-finding methods.

**3.1. Douglas-Rachford Algorithm: the nonexpansive case.** An elementary approach for solving (8) and (9) is to iteratively enforce these equalities with the following update equations:

$$(10) \quad v^{k+1} = 2F(w^k) - w^k$$

$$(11) \quad w^{k+1} = 2H(v^{k+1}) - v^{k+1}.$$

Substituting (10) into (11) gives a single update equation for  $w^k$  in the form

$$w^{k+1} = (2H - I)(2F - I)w^k.$$

In this form, described in [1, Th. 1.48] as a Banach-Picard iteration of the map  $T = (2H - I)(2F - I)$ , the iteration will converge if  $T$  is a contraction mapping on  $\mathbb{R}^n$ .

In fact, as seen in the examples, the iterates of  $T$  may converge, at least locally, even when  $T$  is not a contraction. This local convergence holds for instance when  $T$  is differentiable and all eigenvalues of the Jacobian of  $T$  at the fixed point have absolute value less than 1. In a typical application, the map  $F$  for the forward model has a large number of contracting directions, as this map tries to fit to data. These contracting directions may counterbalance any expanding directions arising from  $H$ , leading to net contraction.

In general, however,  $T$  is not a contraction, even in the case that  $F$  and  $H$  are both proximal maps for proper, convex functions  $f$  and  $h$ , respectively. An alternative algorithm that can be guaranteed to converge when  $F$  and  $H$  are both proximal maps is the Douglas-Rachford splitting algorithm as described in [1, Th. 25.6].

The DR algorithm for our problem is given by

$$(12) \quad v^{k+1} = 2F(w^k) - w^k$$

$$(13) \quad w^{k+1} = (1 - \rho_k)w^k + \rho_k(2H(v^{k+1}) - v^{k+1}),$$

where  $\{\rho_k\}$  is a sequence of positive numbers specified below. Noting that  $2H(v^{k+1}) - v^{k+1} = Tw^k$ , the DR algorithm can also be written as

$$(14) \quad w^{k+1} = w^k + \rho_k(Tw^k - w^k),$$

which is known as the Krasnel'skii-Mann iteration of  $T$ . When both  $F$  and  $H$  are proximal maps, then [1, Th. 25.6] gives a convergence result for the Douglas-Rachford iteration. However, a more general theorem on the Mann iteration gives convergence when  $T$  is non-expansive (i.e., is Lipschitz with Lipschitz constant at most 1), which may be true even when one or both of  $F$  or  $H$  is not a proximal map.

**THEOREM 3.** (*Convergence of DR algorithm*) *Let  $F : \mathbb{R}^n \rightarrow \mathbb{R}^n$  and  $H : \mathbb{R}^n \rightarrow \mathbb{R}^n$  be maps such that  $T = (2H - I)(2F - I)$  is nonexpansive with at least one fixed point. Let  $\rho_k \in [0, 1]$  for each  $k$ , with  $\sum_{k=1}^{\infty} \rho_k(1 - \rho_k) = \infty$ . Then for any  $w^0 \in \mathbb{R}^n$ , the sequence defined by the DR algorithm of (12) and (13) (or equivalently by (14)) converges to a fixed point of  $T$ .*

*Proof.* Apply [1, Th. 5.14]. □

In practice,  $\rho_k$  is often taken to be fixed; we include the general result for varying  $\rho_k$  for completeness. A related method that uses a decreasing sequence of step sizes to guarantee convergence is found in [3].

There are a number of special cases in which the DR algorithm and Theorem 3 are of particular interest. First we note that when  $\rho_k = 1/2$ , then the DR algorithm is exactly the ADMM algorithm with variable splitting as used in [17] and Algorithm 1 of [15]. A proof of this fact is contained in Appendix B. However, we will see in examples that in some cases, a fixed value of  $\rho_k$  other than  $1/2$  gives faster convergence than standard ADMM.

In the special case when both  $F$  and  $H$  are proximal maps, then  $T$  is nonexpansive and the DR algorithm converges to a fixed point of  $T$ . The following corollary records this point.

**COROLLARY 4.** *Let  $F$  and  $H$  both be proximal maps for proper, convex functions  $f$  and  $h$ , respectively, let  $T = (2H - I)(2F - I)$ , and suppose  $T$  has at least one fixed point. Then for any initial point, the DR algorithm defined by (12) and (13) (or equivalently by (14)) converges to a fixed point of  $T$ .*

*Proof.* Since  $F$  and  $H$  are proximal maps,  $2F - I$  and  $2H - I$  are both nonexpansive by [1, Th. 23.10]. Hence  $T$  is nonexpansive and Theorem 3 applies.  $\square$

Of course, it is still possible for the DR-algorithm to converge even when  $F$  and  $H$  are not proximal mappings. For example, Theorem 3 still applies when  $F$  is a proximal map and  $H$  is a denoising operator, as long as  $(2F - I)(2H - I)$  is nonexpansive.

**3.2. Beyond nonexpansive maps.** Theorem 3 gives guaranteed global convergence when  $T$  is nonexpansive and  $\rho_k$  satisfies the conditions given there. However, the DR algorithm may still be convergent even when the assumptions of this theorem are violated. In examples below, we illustrate convergence with  $\rho_k > 1$ , which violates the assumptions of Theorem 3.

More generally, when  $T$  is differentiable at a fixed point, the rate of convergence is closely related to the spectrum of the linearization of  $T$  near this fixed point. Taking a constant value of  $\rho_k = \rho$  in (14) maintains a fixed point at  $w^*$  but changes the linear part to have eigenvalues  $\mu_j = \rho\lambda_j + (1 - \rho)$ , where  $\lambda_1, \dots, \lambda_n$  are the eigenvalues of the linear part of  $T$ . The DR algorithm converges locally exactly when all of these  $\mu_j$  are strictly inside the unit disk in the complex plane. This can be achieved for sufficiently small  $\rho$  precisely when the real part of each  $\lambda_j$  is less than 1. Since there is no constraint on the complex part of the eigenvalues, the map  $T$  may be quite expansive in some directions. In this case, the optimal rate of convergence is obtained when  $\rho$  is chosen so that the eigenvalues  $\mu_j$  all lie within a minimum radius disk about the origin.

**THEOREM 5. (Local convergence of DR algorithm)** *Let  $F : \mathbb{R}^n \rightarrow \mathbb{R}^n$  and  $H : \mathbb{R}^n \rightarrow \mathbb{R}^n$  be maps such that  $T = (2H - I)(2F - I)$  has a fixed point  $w^*$ . Suppose that  $T$  is differentiable at  $w^*$  and that the Jacobian of  $T$  at  $w^*$  has eigenvalues  $\lambda_1, \dots, \lambda_n$  with the real part of  $\lambda_j$  less than 1 for all  $j$ . Then there is  $\rho > 0$  and an open set  $U$  containing  $w^*$  such that for any initial point  $w^0$  in  $U$ , the iterates defined by (14) with each  $\rho_k = \rho$  converge to  $w^*$ .*

The proof of this theorem is given in Appendix A.

When even these more relaxed eigenvalue conditions are not satisfied by the map  $T$ , then the fixed point is typically a saddle point with many contracting directions and a small number of expanding directions. There are a variety of sophisticated algorithms that may be applied to determine the fixed point in such cases, including Jacobian-free Newton Krylov methods. For the moment, we note that if good approximations to the Jacobian derivatives of  $F$  and  $H$  are available, then we may apply Newton's method to obtain superlinear convergence even when the DR algorithm does not converge for any  $\rho$ .

An alternative approach is to convert the CE equations back into an optimization framework by considering the residual error norm given by

$$(15) \quad R(w, v) \triangleq \left( \left\| F(w) - \frac{w+v}{2} \right\|^2 + \left\| H(v) - \frac{w+v}{2} \right\|^2 \right)^{\frac{1}{2}}$$

and minimizing  $R^2(w, v)$  over  $w$  and  $v$ . Assuming that a solution of the CE equations exists, then that solution is also a minimum of this objective function, and under appropriate hypotheses, this objective is convex. Also, the residual error of equation (15) is also useful as a general measure of convergence when computing the CE solution.

Other candidate algorithms include the forward-backward algorithm and related algorithms as presented in [4]. We leave further investigation of efficient algorithms for solving the CE equations to future research.

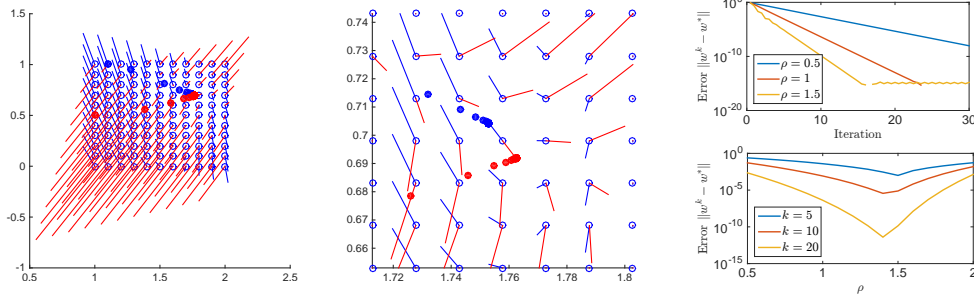


FIG. 1. *Left: Map fields and trajectories for 2-dimensional toy example with  $\rho = 1$ . Blue segments show the map  $v \mapsto H(v)$ , red segments show  $w \mapsto F(w)$ , with open blue circles showing the common endpoints of these maps. Blue and red dots show the points  $v^k$  and  $w^k$ , respectively. Middle: Zoom in near the fixed point of the plot on the left. Right: Top shows the decrease in error as a function of iteration for several values of  $\rho$ . Bottom shows the error as a function of  $\rho$  for several values of the iteration number,  $k$ .*

**4. Experimental Results.** Here we provide some computational examples of varying complexity. Importantly, for each of these examples, the operator  $H$  is not a proximal mapping, so the traditional optimization formulation of equation (1) is not applicable.

We start with a toy model in 2 dimensions to illustrate the ideas, then follow with some more complex examples.

**4.1. Toy model.** The first example uses

$$H(v) = 0.9(v_1 + 0.2, v_2 - 0.2 \sin(2v_1))^T,$$

$$F(w) = (I + \sigma^2 A^T A)^{-1} (w + \sigma^2 A^T y).$$

In this case,  $F$  is a proximal map as in (4) corresponding to  $f(x) = \|Ax - y\|^2/2$  and  $H$  is a weakly contracting map designed to illustrate the behavior of the algorithm. We use  $\sigma = 1$  and

$$A = \begin{bmatrix} 0.3 & 0.6 \\ 0.4 & 0.5 \end{bmatrix}, \quad y = \begin{bmatrix} 1 \\ 1 \end{bmatrix}.$$

We apply the DR algorithm of (12) and (13) with a fixed value of  $\rho$ .

Figure 1 shows the vectors obtained from each of the maps  $F$  and  $H$ . Blue line segments are vectors from a point  $v$  to  $H(v)$ , and red line segments are vectors from a point  $w$  to  $F(w)$ . The starting points of each pair of red and blue vectors are chosen so that they have a common ending point, signified by an open circle. Closed circles show the trajectories of  $v^k$  in blue and  $w^k$  in red. In each case, the trajectories converge to points for which the corresponding red and blue vectors have a common end point and are equal in magnitude and opposite in direction; this is the consensus equilibrium solution. In the right two panels of this figure, we use the true fixed point to plot error versus iterate for several values of  $\rho$  and error versus  $\rho$  for several values of the iteration number,  $k$ . In this case, convergence is robust enough that values of  $\rho$  above 1 give faster convergence than standard ADMM ( $\rho = 1/2$ ). For this example, the linearization of the map in (14) at the fixed point has a maximum eigenvalue of 0.82 when  $\rho = 0.5$ , 0.63 when  $\rho = 1$ , and 0.45 when  $\rho = 1.5$ .

**4.2. Stochastic matrix.** The next example uses the proximal map form for  $F$  as in the previous example, although now with dimension  $n = 100$ .  $A$  and  $y$  were chosen using the random number generator rand in Matlab, approximating the uniform distribution on  $[0, 1]$  in each component. The map  $H$  has the form  $H(v) = Wv$ ; here  $W$  is constructed by first choosing entries at random in the interval  $[0, 1]$  as for  $A$ , then replacing the diagonal entry by

the maximum entry in that row (in which case the maximum entry may appear twice in one row), and then normalizing so that each row sums to 1. This mimics some of the features in a weight matrix appearing in denoisers such as non-local means [2] but is designed to allow us to compute an exact analytic solution of the CE equations. In particular, since  $W$  is not symmetric,  $H$  cannot be a proximal map, as shown in [15].

In order to demonstrate a range of possible convergence behaviors for the DR algorithm, we first fix the matrices  $A$  and  $W$  and the vector  $y$  as above, and then we use a one-parameter family of maps  $H_r(v) = rWv + (1-r)I/2$ . By varying  $r$  from 0.95 to 1.02, we can illustrate important distinct cases of convergence for our method.

As a quick review, recall that if the Lipschitz constant,  $L(T) < 1$ , then the operator  $T$  is a contraction, and if  $L(T) \leq 1$  we say it is nonexpansive. Moreover, for linear operators,  $L(T) = \sigma_{max}$  where  $\sigma_{max}$  is the maximum singular value of  $T$ ; and  $\sigma_{max} \geq |\lambda_{max}|$  where  $\lambda_{max}$  is the eigenvalue with greatest magnitude. Consequently, operators  $T$  with  $L(T) > 1$  may still have eigenvalues that lie strictly within the unit circle.

Below are four simulation cases we study:

- Case 1,  $r = 0.95$ : In this case,  $T$  is nonexpansive, the Lipschitz constant  $L(T) < 1$ , and the mapping is a contraction. Therefore, the conditions of Theorem 3 hold whenever  $\rho \in (0, 1)$ , and the DR algorithm is guaranteed to converge. Interestingly, the plots show convergence even for some  $\rho > 1$ .
- Case 2,  $r = 0.98$ : In this case,  $T$  is not nonexpansive, the Lipschitz constant  $L(T) > 1$ , and the mapping expands in some directions. Therefore, the conditions of Theorem 3 do not hold. Nonetheless, all the eigenvalues of the linear operator  $T$  lie strictly inside unit circle, so the DR algorithm converges locally by Theorem 3. Interestingly, it also converges for some  $\rho > 1$ .
- Case 3,  $r = 1$ : In this case,  $T$  is not nonexpansive, the Lipschitz constant  $L(T) > 1$ , and the conditions of Theorem 3 do not hold. However, since the largest magnitude eigenvalue is given by  $-1.0047$ , the DR algorithm converges locally by Theorem 3 for some  $\rho < 1$  but not for  $\rho = 1$ .
- Case 4,  $r = 1.02$ : In this case,  $T$  is not nonexpansive, the Lipschitz constant  $L(T) > 1$ , and the conditions of Theorem 3 do not hold. The largest magnitude eigenvalue is given by  $1.0185 + 0.0366i$  and in this case the DR algorithm is not convergent for  $\rho > 0$ .

In Figure 2, we plot the norm of the difference between  $w^k$  and the analytic solution  $w^*$ , normalized by the number of pixels, for each of the 4 cases.

In Figure 3, we plot the trajectories in Case 3 for several representative pixels as a function of the iteration number. We also plot the dependence of the convergence on  $\rho$ : the middle right plot shows the error at a fixed number of iterations as a function of  $\rho$ , and the rightmost plot shows the number of iterations needed to achieve a fixed error. The trajectories in Figure 3 show damped oscillations similar to those observed when using non-local means in [15]. These oscillations arise from largest magnitude eigenvalues of  $T$  that are not real. In this case,  $T$  has eigenvalues of  $0.9985 \pm 0.0359i$ .

Note that Theorem 3 applies only to Case 1. However, Theorem 5 applies to all but the last case, which is consistent with the corresponding convergence in all but the last case. We note in passing that we have used Newton's method to find the solution to CE equations even in this divergent case, but we do not further explore such methods and results here.

We note also that not all examples chosen randomly as described above converge, and in not all cases does a value of  $\rho$  larger than 0.5 give faster convergence than  $\rho = 0.5$ . In fact, roughly half of the maps constructed this way diverged, but the vast majority had only one expanding eigenvalue or a pair of complex conjugate expanding eigenvalues. We leave the

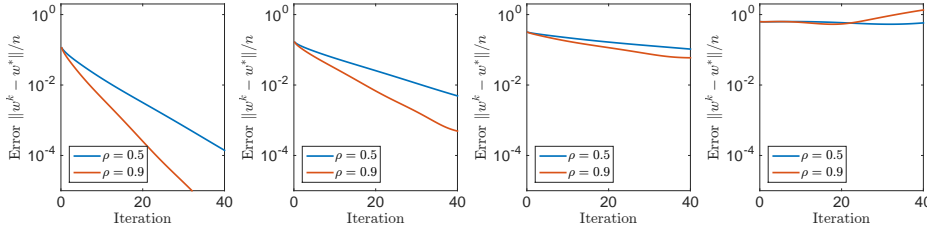


FIG. 2. Error  $\|w^k - w^*\|/n$  versus iteration for cases 1–4. Left: (Case 1)  $T$  is a contraction. Middle left: (Case 2)  $T$  has Lipschitz constant larger than 1 but all eigenvalues are less than 1 in magnitude. Middle right: (Case 3)  $T$  has Lipschitz constant larger than 1 and at least one eigenvalue larger than 1 in magnitude. Right: (Case 4)  $T$  has an eigenvalue with real part larger than 1, and the iterates diverge.

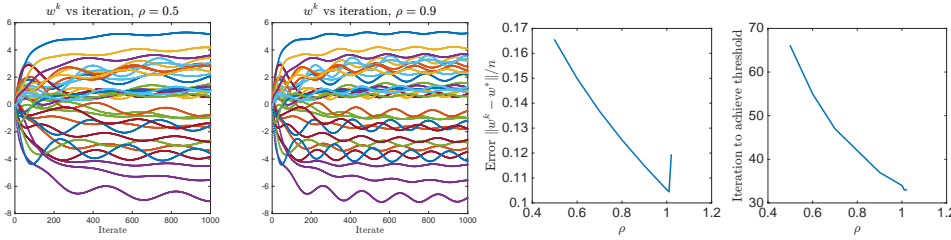


FIG. 3. Case 3 experiments. Left and middle left: Representative components of the vector  $w^k$  versus iterate for two values of  $\rho$ . The damped oscillations visible here are characteristic of nonreal eigenvalues inside the unit circle. Middle right: Error  $\|w^k - w^*\|/n$  as a function of  $\rho$  for fixed  $k = 1000$ . Right: Minimum number of iterations needed for error  $\|w^k - w^*\|/n$  to fall below 0.2.

study of algorithms that converge in this saddle case to future research. For now, these results illustrate that the DR algorithm converges when  $H$  is chosen from an important class of maps that mimic certain denoisers but that are not proximal maps.

**4.3. Sparse Interpolation for Electron Microscopy.** In this section, we present results using our DR algorithm and the consensus equilibrium framework for the problem of computing the sparse interpolation of real transmission electron microscope images. Recently, there has been growing interest in interpolation of sparsely sampled electron microscopy data as a method for both reducing scan time and beam damage as compared to traditional raster scanning methods [9, 15].

Figure 4(a) shows a portion of a densely sampled High Resolution Transmission Electron Microscopy (HR-TEM) image of gold nano-rods taken with an aberration-corrected FEI Titan operating at 300 kV [10]. Images were recorded on a 2k by 2k Gatan Ultrascan CCD at electron optical magnifications ranging from 380kX to 640kX. Figure 4(b) shows a portion of the binary mask formed by randomly selecting 20% of the measured pixels. This mask was applied to the HR-TEM image to generate a simulated sparsely sampled micrograph shown in Figure 4(c). In application, this image would be obtained by sampling only the points in the mask, and thus reducing either beam damage or increasing acquisition speed [7, 8].

The sparsely sampled images were then interpolated using the CE framework of equations 2 and 3, where the forward proximal map,  $F$  is given by the sparse sampling model, and the denoising operator,  $H$ , was given by the BM3D denoising algorithm [5, 6]. The details of how to derive  $F$  are given in [15]; however, the final form of the operator is quite simple and

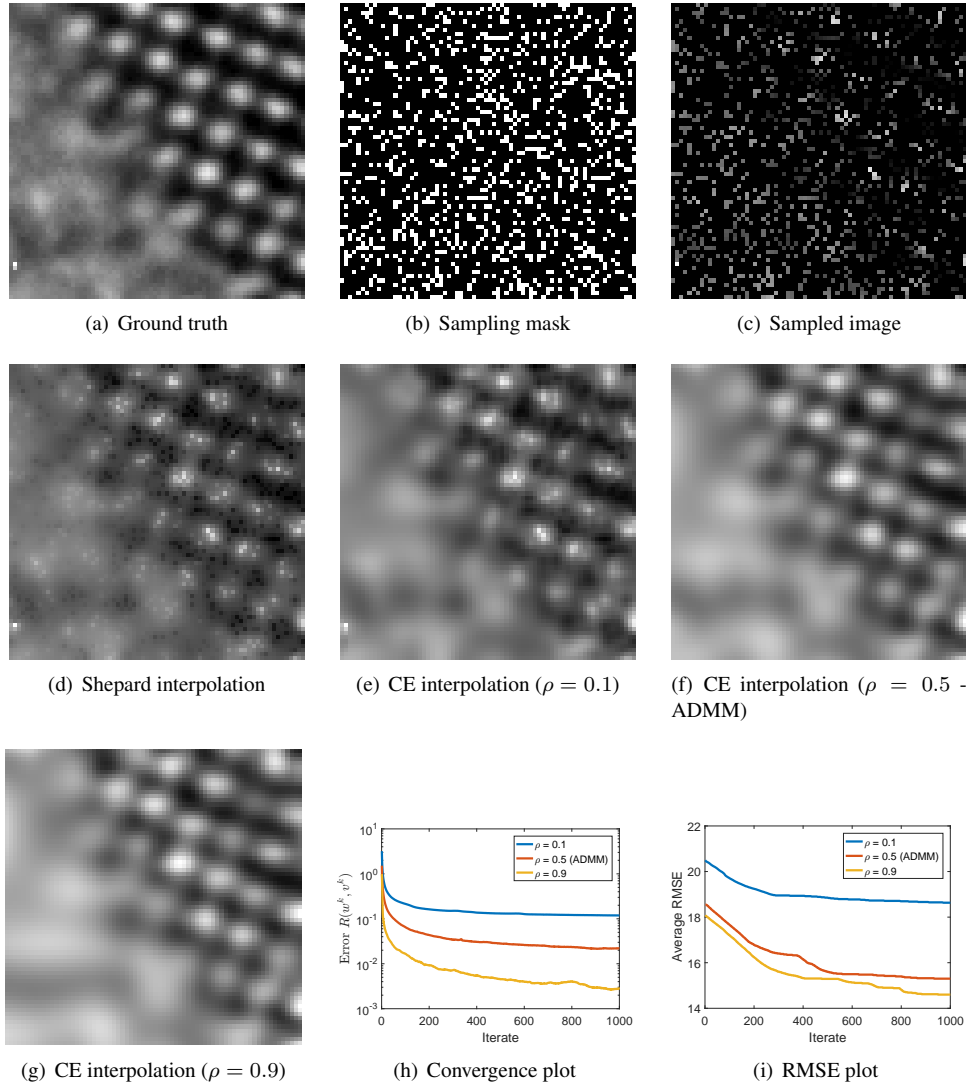


FIG. 4. Sparse interpolation of gold atoms embedded on a carbon nano-substrate, imaged with an aberration-corrected FEI Titan operating at 300 kV. First row: Full resolution ground truth image, sparse mask consisting of 20% of samples, and sampled image at mask locations. Second row: Shepard's interpolation, consensus equilibrium interpolation of the sampled image, using  $\rho = 0.1$  and  $\rho = 0.5$  (corresponding to ADMM). Third row: Consensus equilibrium ( $\rho = 0.9$ ) interpolation; convergence plot comparing the residual norm for  $\rho = 0.1$ ,  $\rho = 0.5$  (ADMM), and  $\rho = 0.9$ ; and average RMSE compared to ground truth versus iteration number. Notice that by setting  $\rho = 0.9$ , the DR algorithm has faster convergence than ADMM (i.e., DR with  $\rho = 0.5$ ) and results in a reconstructions with lower RMSE for the same number of iterations.

given by

$$(16) \quad F_i(w) = \begin{cases} [y_i]_+ & \text{if } y_i \text{ is measured} \\ [w_i]_+ & \text{otherwise,} \end{cases}$$

where  $[\cdot]_+$  represents zeroing of any negative argument and we assume that the added noise

in the sampling process has zero variance<sup>1</sup>. The BM3D denoising software was downloaded directly from Foi’s webpage at <http://www.cs.tut.fi/foi/GCF-BM3D>. We set the denoising strength parameter in the software to 0.3, and the block size to 8.

In order to better quantify our results, convergence plots were computed as ensemble averages taken over interpolations of 10 different non-overlapping images from the same gold atoms dataset, using the same sampling mask for each image. As a measure of convergence, we used both the residual norm of equation (15) and also the average root-mean-squared error (RMSE) as compared to the densely sampled ground-truth image. All HR-TEM images were scaled to the range of  $[0 - 255]$  for comparison. We also used the linear Shepard interpolation algorithm as both an initialization for our algorithm as well as a baseline of comparison [14].

Figures 4 illustrates the results of the experiment. Notice that Figures 4(h) and (i) indicate that with  $\rho = 0.9$  the proposed DR algorithm converges faster than ADMM (i.e., DR with  $\rho = 0.5$ ) both in terms of the residual error and RMSE as compared to ground truth. In fact, even after 1000 iterations, the result achieved by DR with  $\rho = 0.9$  has significantly lower RMSE (on a scale of  $[0 - 255]$ ) than either DR with  $\rho = 0.1$  or ADMM. Notice that this additional distortion is noticeable when comparing Figures 4(e) and (g).

**5. Conclusions.** We present a new framework for image reconstruction, which we term the Consensus Equilibrium (CE), that balances data fitting operations with the actions of general image denoisers. While the CE solution agrees with the conventional regularized inversion in that special case, it also applies in a wide array of problems for which there is no corresponding optimization formulation.

The intuitively appealing property of the CE solution is that it is defined by the balance between two operators rather than the minimum of a cost function. The CE solution is given by the consensus image that arises simultaneously from the operation of an image denoising map applied to image plus noise and a proximal (data fit) map applied to image minus the same noise.

We also propose a family of algorithms for solving the CE equations based on the Douglas-Rachford (DR) algorithm and parameterized by the value  $\rho$ . When  $\rho = 0.5$ , we show that the DR algorithm exactly corresponds to the ADMM algorithm applied in the Plug-and-Play framework. We present some sufficient conditions for convergence of the DR algorithm in the form of two theorems; at the same time, we emphasize that the CE solution may be obtained using any of a number of possible approaches, including root-finding methods and other methods to find fixed points.

Our experimental results, on a variety of problems with varying complexity, demonstrate that our DR algorithm is potentially useful for two reasons. First, it can solve important problems for which there is no corresponding regularized optimization; and second, it can improve convergence speed relative to the ADMM algorithm.

**Acknowledgments.** The authors thank Dr. Lawrence F. Drummy of Air Force Research Lab, for providing the gold atoms TEM dataset.

**A. Appendix: Proofs.**

*Proof of Theorem 1.* For further background on convex analysis, see [11]. Define the cost function

$$c(x) = f(x) + h(x).$$

Suppose first that  $x^*$  is a solution of the CE equations. Since  $c(x)$  is convex, a necessary and sufficient condition for  $x^*$  to belong to the minimum set of  $c$  is that that  $\mathbf{0} \in \partial c(x^*)$ , where

---

<sup>1</sup> In this case, the algorithm results in true interpolation since the measured pixels are reproduced without any modification.

$\partial c(x)$  denotes the subdifferential of  $c(x)$  at  $x$ . That is,  $\partial c(x^*)$  is the set of vectors  $w$  such that  $c(x) \geq c(x^*) + \langle w, x - x^* \rangle$ . For a fixed  $x$ , let  $f_x(v) := f(v) + \|x - v\|^2/(2\sigma^2)$ , and define  $h_x$  analogously for  $h$ . Then  $f_x$  and  $h_x$  are convex as a function of  $v$ . Also, the assumption that

$$F(x^* - u^*) = x^*,$$

implies that  $f_{x^* - u^*}(v)$  takes its minimum at  $v = x^*$ , hence  $\mathbf{0} \in \partial f_{x^* - u^*}(x^*)$ . Likewise,  $\mathbf{0} \in \partial h_{x^* + u^*}(x^*)$ . By [11, Th. 23.8], the assumptions on  $f$  and  $h$  imply that

$$\partial f_{x^* - u^*}(x^*) = \partial f(x^*) + \frac{x^* - (x^* - u^*)}{\sigma^2} = \partial f(x^*) + \frac{u^*}{\sigma^2},$$

and

$$\partial h_{x^* + u^*}(x^*) = \partial h(x^*) + \frac{x^* - (x^* + u^*)}{\sigma^2} = \partial h(x^*) - \frac{u^*}{\sigma^2}.$$

Hence

$$\mathbf{0} \in \partial f_{x^* - u^*}(x^*) + \partial h_{x^* + u^*}(x^*) = \partial f(x^*) + \partial h(x^*).$$

Applying [11, Th. 23.8] to  $c = f + h$ , we have  $\mathbf{0} \in \partial c(x^*)$  and hence  $x^*$  is a global minimum for  $c$ .

For the converse, suppose  $x^*$  is the solution of (1). Again by [11, Th. 23.8], this means that  $\mathbf{0} \in \partial f(x^*) + \partial h(x^*)$ , hence there exists  $u_\sigma^* \in \partial h(x^*)$  with  $-u_\sigma^* \in \partial f(x^*)$ . Let  $u^* = \sigma^2 u_\sigma^*$ , so that  $-u^* \in \sigma^2 \partial f(x^*)$ . By [1, Prop. 16.34],  $F(x) = p$  if and only if  $x - p \in \partial(\sigma^2 f)(p)$ , and by definition of the subgradient, this is the same as  $x - p \in \sigma^2 \partial f(p)$ . Taking  $p = x^*$  and  $x - p = -u^*$ , we have  $x = x^* - u^*$  and hence  $F(x^* - u^*) = x^*$ . Likewise,  $H(x^* + u^*) = x^*$ , so the CE equations are satisfied.  $\square$

*Proof of Theorem 5.* Let  $T_\rho$  denote the map  $(1 - \rho)I + \rho T$ . Let  $\mu_j(\rho) = (1 - \rho) + \rho \lambda_j$  and note that  $T_\rho$  has eigenvalues  $\mu_1, \dots, \mu_n$ . Since the real part of  $\lambda_j$  is less than 1, the line segment defined by  $\mu_j(\rho)$  for  $\rho$  in the interval  $[0, 1]$  has a nonempty intersection with the open unit disk in the complex plane. For each  $j$ , there is some  $\epsilon_j > 0$  so that this intersection contains the set of points  $\mu_j(\rho)$  for  $\rho$  in  $(0, \epsilon_j]$ . Taking  $\epsilon_0$  to be the minimum of the  $\epsilon_j$  and taking  $\rho$  in the interval  $(0, \epsilon_0]$ , there exists  $r < 1$  for which  $|\mu_j(\rho)| \leq r < 1$  for all  $j$ .

For this choice of  $\rho$ , let  $A$  be the Jacobian of  $T_\rho$  at the fixed point,  $w^*$ , which we may assume is the origin. The Schur triangulation gives a unitary matrix  $Q$  and an upper triangular matrix  $U$  with  $U = Q^{-1}AQ$ . Write  $U = \Lambda + \hat{U}$  with  $\Lambda$  diagonal and  $\hat{U}$  zero on the diagonal. Let  $u_{\max}$  be the maximum of  $|\hat{U}_{i,j}|$  over all entries in  $\hat{U}$ . For  $\epsilon > 0$ , define  $D$  to be the diagonal  $n \times n$  matrix with  $D_{i,i} = \epsilon^i$ . A computation shows that  $D^{-1}UD$  has the same diagonal entries as  $U$  but that each off-diagonal has the form  $U_{i,j}\epsilon^{j-i}$  with  $j > i$ , hence is bounded by  $\epsilon u_{\max}$  in norm. This plus the differentiability of  $T_\rho$  implies that for  $x$  in a neighborhood of 0,

$$\begin{aligned} \|D^{-1}Q^{-1}T_\rho Q D x\| &= \|\Lambda x + D^{-1}\hat{U}Dx\| + o(\|x\|) \\ &\leq (r + n\epsilon u_{\max} + R(\|x\|))\|x\|, \end{aligned}$$

where  $R(\|x\|)$  decreases to 0 as  $\|x\|$  tends to 0. Choosing  $\epsilon$  and  $\|x\|$  sufficiently small, we have  $r + n\epsilon u_{\max} + R(\|x\|) < \beta$  for some  $\beta < 1$ . In this case we can iterate to obtain

$$\|D^{-1}Q^{-1}T_\rho^k Q D x\| \leq \beta^k \|x\|.$$

In other words, for  $x^0$  in a neighborhood  $N$  of the origin, the iterates  $x^k = D^{-1}Q^{-1}T_\rho^k Q D x^0$  converge geometrically to the origin. Multiplying by  $QD$  and labeling  $w^k = QDx^k$ , we have  $w^k = T_\rho^k w^0$  converges geometrically to 0 for all  $w^0$  in the neighborhood  $QDN$  of the origin.  $\square$

**B. Appendix: ADMM as a special case of DR.** In [15], the ADMM algorithm was used to find the minimum of  $f_1 + f_2$ , where  $f_1$  and  $f_2$  are both appropriate convex functions, using the corresponding proximal maps  $F_1$  and  $F_2$ . In this form, the ADMM algorithm is given by

$$(17) \quad a^{k+1} = F_1(b^k - c^k)$$

$$(18) \quad b^{k+1} = F_2(a^{k+1} + c^k)$$

$$(19) \quad c^{k+1} = c^k + a^{k+1} - b^{k+1}$$

In order to show the equivalence of this ADMM algorithm with the DR algorithm with  $\rho_k = 1/2$  for all  $k$  as described above, we introduce new variables  $p^k = b^k - c^k$  and  $q^k = b^k + c^k$ . In this case  $b^k = (p^k + q^k)/2$  and  $c^k = (q^k - p^k)/2$ . Using  $q^{k+1} = b^{k+1} + c^{k+1}$  in (19) gives  $q^{k+1} = c^k + a^{k+1}$ , hence (18) gives  $b^{k+1} = F_2(q^{k+1})$ . Also, (17) implies that  $a^{k+1} = F_1(p^k)$ , so  $q^{k+1} = c^k + F_1(p^k)$ . Expressed in  $p$  and  $q$ , these expressions for  $b^{k+1}$  and  $q^{k+1}$  yield the system

$$(20) \quad p^{k+1} = 2F_2(q^{k+1}) - q^{k+1}$$

$$(21) \quad q^{k+1} = \frac{1}{2}q^k + \frac{1}{2}(2F_1(p^k) - p^k).$$

Renaming and reindexing with  $v^k = p^k$  and  $w^k = q^{k+1}$  (hence  $w^{k+1} = q^{k+2}$ ) gives

$$(22) \quad v^{k+1} = 2F_2(w^k) - w^k$$

$$(23) \quad w^{k+1} = \frac{1}{2}w^k + \frac{1}{2}(2F_1(v^{k+1}) - v^{k+1}),$$

which is the same as (12) and (13) with  $F_1 = H$  and  $F_2 = F$  and  $\rho_k = 1/2$ .

#### REFERENCES

- [1] H. H. BAUSCHKE AND P. L. COMBETTES, *Convex analysis and monotone operator theory in Hilbert spaces*, CMS Books in mathematics, Springer, New York, Dordrecht, Heidelberg, 2011.
- [2] A. BUADES, B. COLL, AND J.-M. MOREL, *A review of image denoising algorithms, with a new one*, Multi-scale Modeling & Simulation, 4 (2005), pp. 490–530.
- [3] S. H. CHAN, X. WANG, AND O. A. ELGENDY, *Plug-and-play ADMM for image restoration: Fixed point convergence and applications*, CoRR, abs/1605.01710 (2016), <http://arxiv.org/abs/1605.01710>.
- [4] P. L. COMBETTES AND J.-C. PESQUET, *Proximal splitting methods in signal processing*, in Fixed-point algorithms for inverse problems in science and engineering, Springer New York, 2011, pp. 185–212.
- [5] K. DABOV, A. FOI, V. KATKOVNIK, AND K. EGIАЗARIAN, *Image denoising by sparse 3-D transform-domain collaborative filtering*, IEEE Transactions on Image Processing, 16 (2007), pp. 2080–2095, doi:10.1109/TIP.2007.901238.
- [6] K. DABOV, A. FOI, V. KATKOVNIK, AND K. EGIАЗARIAN, *Image denoising by sparse 3-d transform-domain collaborative filtering*, IEEE Transactions on image processing, 16 (2007), pp. 2080–2095.
- [7] R. EGERTON, P. LI, AND M. MALAC, *Radiation damage in the tem and sem*, Micron, 35 (2004), pp. 399–409.
- [8] A. C. GEIGER, J. A. NEWMAN, S. SREEHARI, S. Z. SULLIVAN, C. A. BOUMAN, AND G. J. SIMPSON, *Sparse sampling image reconstruction in lissajous trajectory beam-scanning multiphoton microscopy*, in SPIE BiOS, International Society for Optics and Photonics, 2017, pp. 1007606–1007606.
- [9] S. HWANG, C. W. HAN, S. V. VENKATAKRISHNAN, C. A. BOUMAN, AND V. ORTALAN, *Towards the low-dose characterization of beam sensitive nanostructures via implementation of sparse image acquisition in scanning transmission electron microscopy*, Measurement Science and Technology, 28 (2017), p. 045402.
- [10] K. PARK, L. F. DRUMMY, R. C. WADAMS, H. KOERNER, D. NEPAL, L. FABRIS, AND R. A. VAIA, *Growth mechanism of gold nanorods*, Chemistry of Materials, 25 (2013), pp. 555–563.
- [11] R. ROCKAFELLAR, *Convex Analysis*, Princeton, N.J. : Princeton University Press, 1997, c1970.
- [12] Y. ROMANO, M. ELAD, AND P. MILANFAR, *The little engine that could: Regularization by denoising (RED)*, CoRR, abs/1611.02862 (2016), <http://arxiv.org/abs/1611.02862>.

- [13] A. ROND, R. GIRYES, AND M. ELAD, *Poisson inverse problems by the plug-and-play scheme*, Journal on Mathematical Imaging and Vision, (2016), <https://arxiv.org/pdf/1511.02500.pdf>.
- [14] D. SHEPARD, *A two-dimensional interpolation function for irregularly-spaced data*, in Proceedings of the 1968 23rd ACM national conference, ACM, 1968, pp. 517–524.
- [15] S. SREEHARI, S. VENKATAKRISHNAN, B. WOHLBERG, G. BUZZARD, L. DRUMMY, J. SIMMONS, AND C. BOUMAN, *Plug-and-play priors for bright field electron tomography and sparse interpolation*, IEEE Transactions on Computational Imaging, (2016).
- [16] S. SREEHARI, S. V. VENKATAKRISHNAN, K. L. BOUMAN, J. P. SIMMONS, L. F. DRUMMY, AND C. A. BOUMAN, *Multi-resolution data fusion for super-resolution electron microscopy*, CoRR, abs/1612.00874 (2016), <http://arxiv.org/abs/1612.00874>.
- [17] S. V. VENKATAKRISHNAN, C. A. BOUMAN, AND B. WOHLBERG, *Plug-and-play priors for model based reconstruction*, in IEEE Global Conference on Signal and Information Processing (GlobalSIP), 2013, IEEE, 2013, pp. 945–948.
- [18] S. V. VENKATAKRISHNAN, L. F. DRUMMY, M. DE GRAEF, J. P. SIMMONS, AND C. A. BOUMAN, *Model based iterative reconstruction for bright field electron tomography*, in IS&T/SPIE Electronic Imaging, International Society for Optics and Photonics, 2013, pp. 86570A–86570A.